

Unobscured central broad line regions in Type-1.9 AGN SDSS J1241+2602

XUEGUANG ZHANG^{*1}

¹Guangxi Key Laboratory for Relativistic Astrophysics, School of Physical Science and Technology, Guangxi University, Nanning, 530004, P. R. China

Submitted to ApJ

ABSTRACT

In this manuscript, strong evidence is reported to support unobscured broad line regions (BLRs) in Type-1.9 AGN SDSS J1241+2602 with reliable broad H α but no broad H β . Commonly, disappearance of broad H β can be explained by the AGN unified model expected heavily obscured BLRs in Type-1.9 AGN. Here, based on properties of two kinds of BH masses, the virial BH mass and the BH mass through the $M_{\text{BH}} - \sigma$ relation, an independent method is proposed to test whether are there unobscured central BLRs in a Type-1.9 AGN. By the reliable measurement of stellar velocity dispersion about $110 \pm 12 \text{ km/s}$ through the host galaxy absorption features in SDSS J1241+2602, the BH mass through the $M_{\text{BH}} - \sigma$ relation is consistent with the virial BH mass $(3.43 \pm 1.25) \times 10^7 M_{\odot}$ determined through properties of the observed broad H α without considering effects of obscurations in SDSS J1241+2602. Meanwhile, if considering heavily obscured BLRs in SDSS J1241+2602, the reddening corrected virial BH mass is tens of times larger than the $M_{\text{BH}} - \sigma$ expected value, leading SDSS J1241+2602 to be an outlier in the $M_{\text{BH}} - \sigma$ space with confidence level higher than 5σ . Therefore, the unobscured BLRs are preferred in the Type-1.9 AGN SDSS J1241+2602. The results indicate that it is necessary to check whether unobscured central BLRs are common in Type-1.9 AGN, when to test the AGN unified model of AGN by properties of Type-1.9 AGN.

Keywords: galaxies:active - galaxies:nuclei - quasars:emission lines - quasars: individual (SDSS J1241+2602)

1. INTRODUCTION

Both broad emission lines from central broad emission line regions (BLRs) and narrow emission lines from extended narrow emission line regions (NLRs) are fundamental spectroscopic characteristics in optical band of Type-1 AGN (broad emission line AGN) (Osterbrock & Mathews 1986; Sulentic et al. 2000; Oh et al. 2015). Meanwhile, strong narrow emission lines from central NLRs but no apparent broad emission lines are fundamental spectroscopic characteristics of Type-2 AGN (narrow emission line AGN). The well-known AGN unified model (Antonucci 1993; Netzer 2015; Balokovic et al. 2018; Kuraszkiewicz et al. 2021; Zhang 2022a) has been hypothesized to explain the different spectroscopic phenomena between Type-1 AGN and Type-2 AGN, after mainly considering severe obscurations on central BLRs in Type-2 AGN. Under the framework of the AGN unified model, Type-2 AGN and Type-1 AGN have intrinsically similar fundamental structures of central accretion disks around

black holes (BHs), BLRs, dust torus and NLRs, but Type-2 AGN have central accretion disks around BHs and BLRs heavily obscured by central dust torus due to orientation with respect to the line of sight. The AGN unified model has been strongly supported by clearly detected polarized broad emission lines and/or clearly detected broad infrared emission lines in some Type-2 AGN (Tran 2003; Savic et al. 2018; Moran et al. 2020).

However, even considering different properties of both central dust torus and central BH accreting process expected properties, some challenges to the AGN unified model have been reported. Franceschini et al. (2002) have discussed probably different evolutionary patterns in Type-1 and Type-2 AGN. Villarroel & Korn (2014) have reported different neighbours around Type-1 and Type-2 AGN. Zou et al. (2019) have reported lower host galaxy stellar masses in X-ray selected Type-1 AGN than Type-2 AGN. Bornancini & Garcia Lambas (2020) have shown significantly different properties of UV/optical and mid-infrared colour distributions of different AGN types. More recently, Zhang (2022b) have shown that direct measurements of stellar velocity dispersion can lead to statistically larger stellar ve-

locity dispersions in Type-1 AGN than in Type-2 AGN, with a confidence level higher than 10σ , even after considering the necessary effects of different redshift and different physical properties related to central BH accreting processes in AGN. As discussed in [Netzer \(2015\)](#), the AGN unified model has been successfully applied to explain different observed spectroscopic features between Type-1 and Type-2 AGN in many different ways, however, the AGN family with many other features considering the reported challenges to the AGN unified model are far from homogeneous.

Besides Type-1 AGN and Type-2 AGN expected by the AGN unified model, there is a special kind of optically selected AGN, Type-1.9 AGN (firstly discussed in [Osterbrock \(1981\)](#)), which have apparent broad $H\alpha$ but no apparent broad $H\beta$. Commonly, disappearance of broad $H\beta$ (or quite large broad Balmer decrements, large flux ratio of broad $H\alpha$ to broad $H\beta$) in Type-1.9 AGN are mainly attributed heavily obscured central BLRs, and can be applied to test the AGN unified model. However, as discussed in [Kwan & Krolik \(1981\)](#); [Canfield & Puetter \(1981\)](#); [Goodrich \(1990\)](#), BLRs modeled with relatively low optical depths and low ionization parameters can reproduce large broad Balmer decrements in Type-1.9 AGN, indicating there are rare Type-1.9 AGN of which central BLRs with large broad Balmer decrements are intrinsic but not due to serious obscuration. [Barcons et al. \(2003\)](#) have discussed that the H1320+551 (a Type-1.9 AGN) with no apparent broad $H\beta$ but apparent and strong broad $H\alpha$ is not consistent with being an obscured Type-1 AGN, through its unabsorbed X-ray properties. More recently, [Hernandez-Garcia et al. \(2017\)](#) have discussed that Type-1.9 AGN and Type-2 AGN have different different variability properties in the UV and X-ray domains, indicating pure obscurations on central regions should be disfavored to explain different features between Type-1.9 AGN and Type-1/2 AGN. Here, in the manuscript, a Type-1.9 AGN, SDSS J124131.46+260233.57 (=SDSS J1241+2602), is interestingly and firstly reported on its unobscured central BLRs with strong evidence from optical spectroscopic results.

The manuscript is organized as follows. Section 2 shows the main hypotheses. Section 3 presents the spectroscopic results of SDSS J1241+2602 at redshift 0.0159. Section 4 describes our necessary discussions. Section 5 gives our final conclusions. And we have adopted the cosmological parameters of $H_0 = 70\text{km} \cdot \text{s}^{-1}\text{Mpc}^{-1}$, $\Omega_\Lambda = 0.7$ and $\Omega_m = 0.3$.

2. MAIN HYPOTHESES

In order to test heavily obscured central BLRs in a Type-1.9 AGN, properties of virial BH mass can be applied as follows.

Accepted the virialization assumption to central BLRs as discussed in [Vestergaard \(2002\)](#); [Peterson et al. \(2004\)](#); [Shen et al. \(2011\)](#), virial BH mass of a broad line AGN can

be conveniently estimated by

$$\frac{M_{BH}}{1.2131 \times 10^{-3} M_\odot} = 5.5 \times \frac{R_{BLRs}}{100\text{light-days}} \times \left(\frac{\sigma}{1000\text{km/s}}\right)^2 \quad (1)$$

, with $G = 6.672 \times 10^{-11}\text{Nm}^2/\text{kg}^2$ as the gravitational constant and R_{BLRs} in units of 100light-days as distance of BLRs to central BH and σ in units of km/s as line width (second moment) of broad emission lines to trace rotating velocities of broad line emission clouds in BLRs. The factor 5.5 is the virial factor, discussed in [Onken et al. \(2004\)](#); [Woo et al. \(2010\)](#); [Graham et al. \(2011\)](#); [Park et al. \(2012\)](#); [Woo et al. \(2015\)](#). And, the R_{BLRs} can be simply estimated through continuum luminosity by the improved empirical relation in [Bentz et al. \(2013\)](#) after necessary corrections of host galaxy contaminations. Moreover, considering strong linear correlation between continuum luminosity and broad $H\alpha$ luminosity as discussed in [Greene & Ho \(2005\)](#); [Mejia-Restrepo et al. \(2022\)](#), virial BH mass of a broad line AGN can be estimated by line width (second moment, $\sigma_{H\alpha}$) and line luminosity ($L_{H\alpha}$) of broad $H\alpha$

$$M_{BH} = 15.6 \times 10^6 \left(\frac{L_{H\alpha}}{10^{42}\text{erg/s}}\right)^{0.55} \left(\frac{\sigma_{H\alpha}}{1000\text{km/s}}\right)^{2.06} M_\odot \quad (2)$$

in order to ignore effects of uncertainties of measured continuum luminosities in broad line AGN with strong host galaxy contributions. Here, the second moment rather than the full width of maximum (FWHM) of broad $H\alpha$ is applied, mainly due to few effects of sharp features around peak of broad line profile on calculated second moment.

Meanwhile, through measured stellar velocity dispersions of host galaxy stellar bulges, the $M_{BH} - \sigma$ relation discussed in [Ferrarese & Merritt \(2000\)](#); [Gebhardt et al. \(2000\)](#); [Kormendy & Ho \(2013\)](#); [Batiste et al. \(2017\)](#); [Bennert et al. \(2021\)](#) can also be conveniently applied to estimate central BH mass in both quiescent galaxies and active galaxies, without effects of obscurations on central BLRs. If there were intrinsically serious obscurations on central BLRs leading to disappearance of broad $H\beta$ in a Type-1.9 AGN, virial BH mass of the Type-1.9 AGN through properties of observed broad $H\alpha$ should be significantly smaller than the $M_{BH} - \sigma$ relation expected value, which is the main point to test obscured/unobscured BLRs in a Type-1.9 AGN. In the next Section, stellar velocity dispersion of SDSS J1241+2602 can be measured through apparent absorption features, leading to measured $M_{BH} - \sigma$ relation determined BH mass of SDSS J1241+2602. Therefore, in SDSS J1241+2602, interesting results are reported and discussed in the following sections on properties of $M_{BH} - \sigma$ relation determined BH mass and on properties of virial BH mass with and without considerations of obscurations on central BLRs.

3. SPECTROSCOPIC RESULTS OF THE TYPE-1.9 AGN SDSS J1241+2602

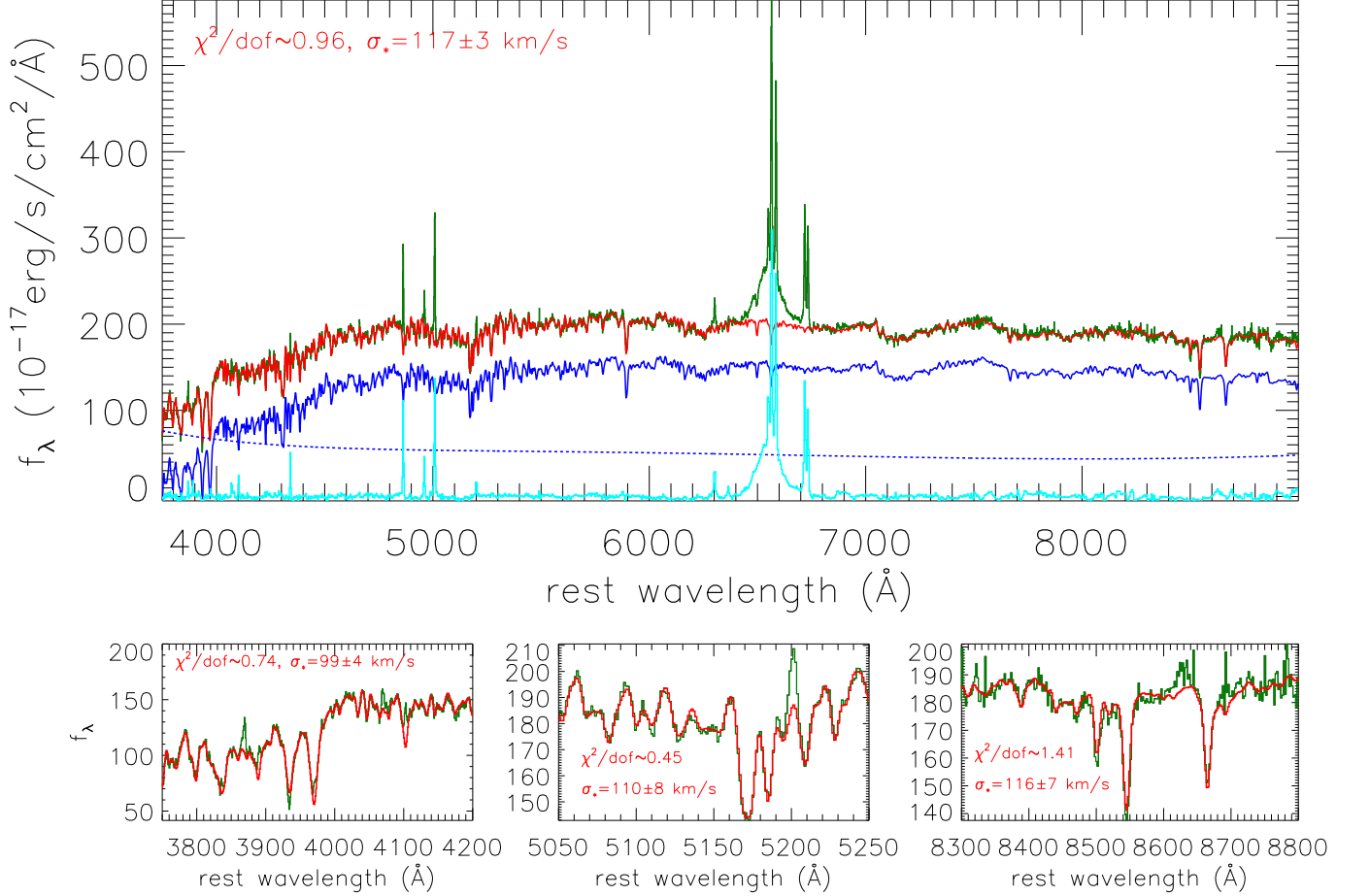


Figure 1. Top panel shows the SSP method determined the best descriptions (solid red line) to the SDSS spectrum (solid dark green line) with emission lines being masked out. In top panel, solid blue line and dashed blue line show the determined host galaxy contributions and the determined AGN continuum emissions, respectively, solid cyan line shows the line spectrum calculated by the SDSS spectrum minus the sum of host galaxy contributions and AGN continuum emissions. Bottom panels show the best fitting results (solid red line) to absorption features (solid dark green line) of the Ca II H+K (left panel), the Mg I (middle panel), the Ca T (right panel). In each panel, the determined χ^2/dof and stellar velocity dispersion are marked in red characters.

SDSS J1241+2602 has its SDSS spectrum (plate-mjd-fiberid=2660-54504-0446) with signal-to-noise about 56 shown in Fig. 1 with apparent broad H α and apparent stellar absorption features. In order to measure the emission lines, the commonly accepted SSP (Simple Stellar Population) method is applied to determine host galaxy contributions. More detailed descriptions on the SSP method can be found in Bruzual & Charlot (2003); Kauffmann et al. (2003); Cid Fernandes et al. (2005); Cappellari (2017). The SSP method has been applied in our previous papers Zhang (2021,a,b, 2022a,b). Here, we show simple descriptions on SSP method as follows. The 39 simple stellar population templates from Bruzual & Charlot (2003); Kauffmann et al. (2003) have been exploited, which can be used to describe the characteristics of almost all the SDSS galaxies. Meanwhile, there is an additional 5th-order polynomial component

applied to describe intrinsic AGN continuum emissions. Here, as shown properties of the composite spectrum of SDSS quasars in Vanden Berk et al. (2001), AGN continuum emissions can be fitted by two power laws with a break at 5000 \AA , indicating a simple power law component not preferred. And moreover, higher-order polynomial functions are also checked, leading to none variability of the following determined χ^2/dof with χ^2 as the summed squared residuals and dof as degrees of freedom. Therefore, a 5th-order polynomial component is preferred in the manuscript. When the SSP method is applied, optical narrow emission lines are masked out by the full width at zero intensity (FWZI) about 450km s $^{-1}$, and the spectrum with rest wavelength range from 6250 to 6750 \AA are also masked out due to the strongly broad H α . Then, through the Levenberg-Marquardt least-squares minimization technique (the known MPFIT package),

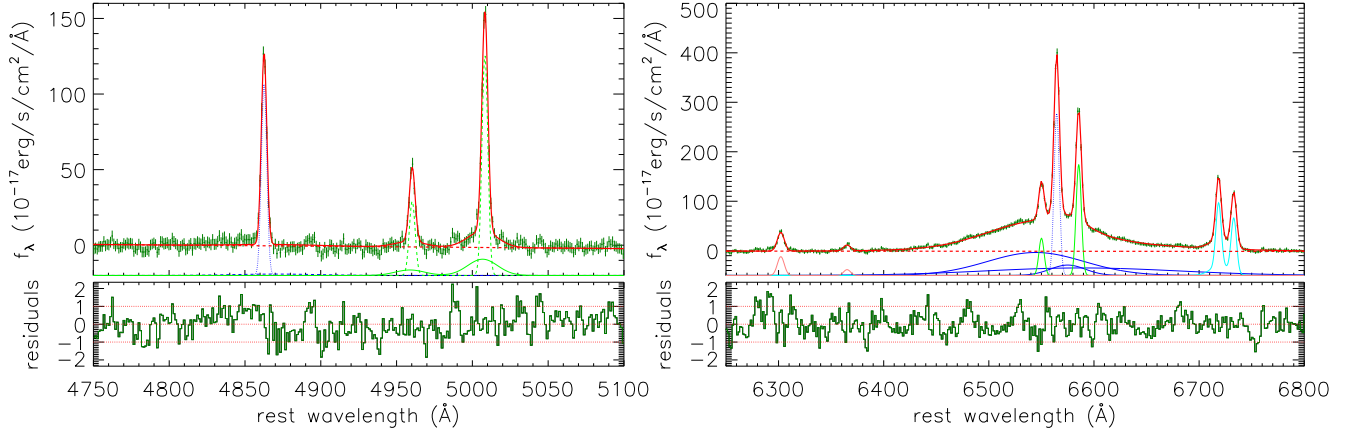


Figure 2. Top panels show the best fitting results (solid red line) to the emission lines in the line spectrum (solid dark green line), and bottom panels show the corresponding residuals calculated by the line spectrum minus the best fitting results and then divided by uncertainties of the SDSS spectrum. In top left panel, dotted blue line shows the narrow H β , dotted and solid green lines show the core components and blue-shifted wings in [O III] doublet. In top right panel, dotted blue line shows the narrow H α , solid blue lines show the determined three broad Gaussian components in broad H α , solid line in green, in pink and in cyan show the [N II] doublet, the [O I] doublet and the [S II] doublet. In each top panel, dashed red line shows the baseline $f_\lambda = 0$. In each bottom panel, horizontal dashed lines show residuals = 0, ± 1 , respectively.

the SDSS spectrum with emission lines being masked out can be described and shown in Fig. 1 with corresponding $\chi^2/dof \sim 0.96$ and with the determined stellar velocity dispersion about 117 ± 3 km/s and with the determined continuum luminosity at rest wavelength 5100 Å (from the determine 5th-order polynomial component) about $(1.09 \pm 0.09) \times 10^{42}$ erg/s.

Before proceeding further, one point is noted. The SDSS pipeline reported stellar velocity dispersion is about 144 ± 3 km/s in SDSS J1241+2602, without considering AGN continuum emissions in the pipeline. If the 5th-order polynomial component is not considered, the similar procedure applied to describe the SDSS spectrum with only narrow emission lines being masked out can lead the determined stellar velocity dispersion to be 146 ± 3 km/s consistent with SDSS pipeline reported value. However, considering the apparent broad H α in SDSS J1241+2602, the 5th-order polynomial component should be preferred.

Moreover, the Ca II triplet (Ca T) from 8300 Å to 8800 Å, the Ca II H+K absorption features from 3750 Å to 4200 Å and the Mg I absorption features from 5050 Å to 5250 Å are applied to re-measure the stellar velocity dispersions of SDSS J1241+2602, through the same SSP method discussed above to describe the whole SDSS spectrum. The best fitting results are shown in the bottom panels of Fig. 1 with the determined stellar velocity dispersions in units of km/s about 116 ± 7 , 99 ± 4 and 110 ± 8 through the Ca T, the Ca II H+K and the Mg I absorption features, respectively. Therefore, in the manuscript, the mean value $\sigma_\star = 110 \pm 12$ km/s is accepted as the stellar velocity dispersion of SDSS J1241+2602.

After subtractions of the host galaxy contributions and the AGN continuum emissions, emission lines in the line spectrum can be measured, similar as what we have previ-

ously done in Zhang (2021a,b, 2022a,b,c). For the emission lines within the rest wavelength range from 4750 Å to 5100 Å, there is one Gaussian function applied to describe narrow H β , four Gaussian functions applied to describe [O III] $\lambda 4959, 5007$ Å doublet (two for the core components, and two for the blue-shifted wings). When the Gaussian functions above are applied, only two criteria are accepted. First, each Gaussian component has line intensity not smaller than zero. Second, the core (blue-shifted) components of the [O III] doublet have the same redshift and the same line width, and have the flux ratio to be fixed to the theoretical value 3. Then, through the Levenberg-Marquardt least-squares minimization technique, the best fitting results to the emission lines and the corresponding residuals (calculated by the line spectrum minus the best fitting results then divided by the uncertainties of the SDSS spectrum) are shown in left panels of Fig. 2 with $\chi_0^2/dof_0 = 209.8/344 \sim 0.61$. Besides the discussed Gaussian components, one additional broad Gaussian function was tried to be applied to describe probable broad H β , however, the fitting procedure led the additional broad component to have the determined line flux and line width smaller than their corresponding determined uncertainties. Therefore, it is not necessary to consider broad Gaussian components to describe the broad H β in SDSS J1241+2602.

Meanwhile, emission lines within the rest wavelength range from 6250 Å to 6800 Å can also be measured by multiple Gaussian functions. There is one Gaussian function applied to describe the narrow H α , three broad Gaussian functions applied to describe the broad H α , two Gaussian functions applied to describe the [N II] doublet, two Gaussian functions applied to describe the [O I] doublet, four Gaussian functions applied to describe the [S II] doublet (two for the core com-

ponents and two for the shifted wings). When the Gaussian functions above are applied, only three criteria are accepted. First, each Gaussian component has line intensity not smaller than zero. Second, the components of the [N II] (the [O I], the [S II]) doublet have the same redshift and the same line width, and the [N II] doublet have the flux ratio to be fixed to the theoretical value 3. Third, the components in the narrow H α and in the narrow H β have the same redshift and the same line width. Then, through the Levenberg-Marquardt least-squares minimization technique, the best fitting results and the corresponding residuals are shown in right panels of Fig. 2 with $\chi^2/dof = 160.6/398 \sim 0.41$. Besides the discussed Gaussian components above, additional Gaussian functions were tried to be applied to describe probable blue/red-shifted wings of the [O I] and the [N II] doublets, however, the fitting procedure led the determined line fluxes of the additional Gaussian components to be smaller than their corresponding determined uncertainties. Therefore, it is not necessary to consider additional blue/red-shifted wings in the [O I] and the [N II] doublets in SDSS J1241+2602.

Before proceeding further, one point is noted. If different numbers (not three) of broad Gaussian functions were applied to describe the broad H α of SDSS J1241+2602, whether were there different results on line profiles? In order to test effects of applications of different numbers of broad Gaussian functions, the F-test technique is applied, similar as what we have recently done in Zhang (2022c). For one, two and four broad Gaussian functions applied to describe broad H α of SDSS J1241+2602, the corresponding χ^2/dof are about $\chi_1^2/dof_1 = 238.8/404 \sim 0.59$, $\chi_2^2/dof_2 = 224.2/401 \sim 0.56$ and $\chi_4^2/dof_4 = 160.6/395 \sim 0.406$, respectively. Then, based on the different χ^2 and dof for different model functions, the F-test technique can be applied to confirm the confidence level higher than 5σ to support that three broad Gaussian functions are referred to describe the broad H α than one or two broad Gaussian functions, and the F-test technique can be applied to confirm the probability only about 10^{-5} to support that the four broad Gaussian functions are preferred to describe the broad H α than the three broad Gaussian functions. Therefore, in the manuscript, three broad Gaussian functions are applied to describe the broad H α of SDSS J1241+2602.

Based on the measured line parameters listed in Table 1, the observed line luminosities are $(3.39 \pm 0.11) \times 10^{39}$ erg/s and $(1.18 \pm 0.02) \times 10^{40}$ erg/s for the narrow H β and the narrow H α , respectively, leading to normal flux ratio 3.5 of the narrow H α to the narrow H β . The line width is about 114 ± 2 km/s for the narrow emission lines, consistent with the measured stellar velocity dispersion. The line luminosity and the line width (second moment) of the broad H α (summed the three broad Gaussian components) are about $(5.69 \pm 0.91) \times 10^{40}$ erg/s and about 3150 ± 420 km/s, respectively. The uncertainties above are determined through the determined uncertainties of the

Table 1. Line parameters of each Gaussian emission component

line	λ_0	σ	flux
Broad H α	6545.8 \pm 2.9	45.6 \pm 2.5	5342 \pm 832
	6575.3 \pm 1.9	16.2 \pm 2.1	839 \pm 196
	6582.1 \pm 12.4	95.9 \pm 13.7	3787 \pm 557
Narrow H α	6564.6 \pm 0.1	2.5 \pm 0.1	2072 \pm 38
Narrow H β	4862.6 \pm 0.1	1.9 \pm 0.1	594 \pm 17
[O III] λ 5007 \AA	5008.3 \pm 0.1	1.9 \pm 0.1	710 \pm 25
	5006.7 \pm 1.1	9.1 \pm 1.3	270 \pm 34
[O I] λ 6300 \AA	6302.1 \pm 0.2	3.3 \pm 0.2	317 \pm 18
[O I] λ 6363 \AA	6365.2 \pm 0.2	3.4 \pm 0.7	105 \pm 18
[N II] λ 6583 \AA	6585.5 \pm 0.1	2.5 \pm 0.1	1406 \pm 32
[S II] λ 6716 \AA	6718.5 \pm 0.1	2.5 \pm 0.1	809 \pm 54
	6719.8 \pm 1.7	9.2 \pm 1.9	446 \pm 81
[S II] λ 6731 \AA	6733.1 \pm 0.1	2.6 \pm 0.1	707 \pm 46
	6734.4 \pm 1.9	9.2 \pm 1.9	3 \pm 2

NOTE—The first column shows which line is measured. The Second, third, fourth columns show the measured line parameters: the center wavelength λ_0 in units of \AA , the line width (second moment) σ in units of \AA and the line flux in units of 10^{-17} erg/s/cm 2 .

For broad H α , there are three Gaussian components. For [O III] λ 5007 \AA and each [S II] emission line, there are two components: the core and the shifted-wing related extended components.

Gaussian emission components. The results can be applied to confirm that SDSS J1241+2602 is a Type-1.9 AGN with apparent broad H α but no broad H β .

4. UNOBSURED CENTRAL BLRS IN THE TYPE-1.9 AGN SDSS J1241+2602

Based on the calculated line width (second moment) and line luminosity of the broad H α without considering any obscurations on central BLRs, the virial BH mass in SDSS J1241+2602 can be estimated as $(3.43 \pm 1.25) \times 10^7 M_\odot$ through equation (2) above. The uncertainty of virial BH mass is estimated by uncertainties of the line width and the line luminosity of the broad H α . Meanwhile, similar virial BH mass about $2.5 \times 10^7 M_\odot$ in SDSS J1241+2602 have been reported in Liu et al. (2019); Martin-Navarro, Shankar & Mezcua (2022). It is interesting that the virial BH mass is consistent with the $M_{\text{BH}} - \sigma$ relation expected BH mass. The dependence of virial BH mass on stellar velocity dispersion in SDSS J1241+2602 is shown in Fig. 3 with previous reported results in the literature for quiescent galaxies, active galaxies and also in Tidal disruption events (TDEs), etc.. The corresponding reference can be found in the caption of Fig. 3.

Before proceeding further, it is interesting to check whether a broad component related to shifted wings of narrow Balmer lines can also lead to so large virial BH mass. If accepted that the broad components shown in Fig. 2 and listed in Table 1

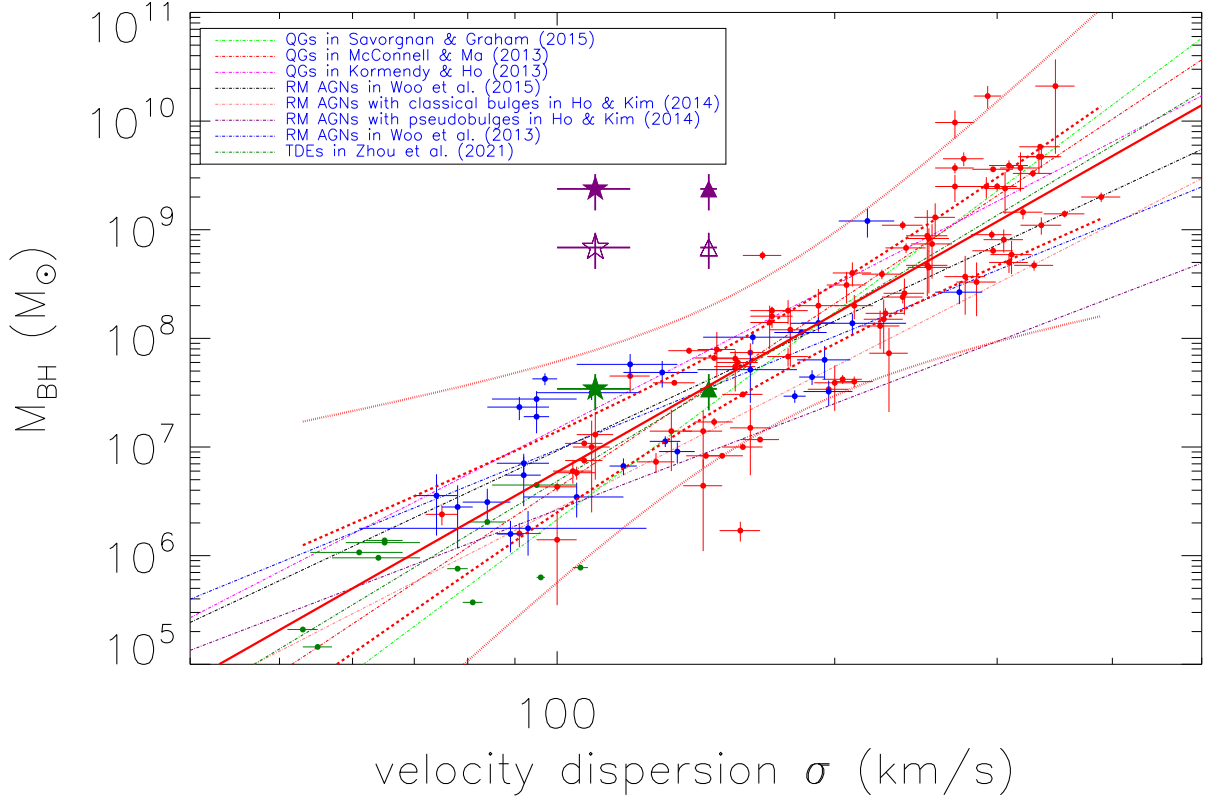


Figure 3. On the correlation between stellar velocity dispersion measured through the absorption features and the virial BH mass of SDSS J1241+2602. Solid five-point-star in dark green shows the virial BH mass of SDSS J1241+2602 determined by properties of the observed broad $H\alpha$ without considerations of any obscurations on central BLRs. Solid and open five-point-star in purple show the virial BH mass of SDSS J1241+2602 determined by properties of the reddening corrected broad $H\alpha$ with $E(B - V) \sim 3.4$ (3σ confidence level for upper limit of broad $H\beta$) and $E(B - V) \sim 2.6$ (5σ confidence level for upper limit of broad $H\beta$), respectively. Dot-dashed lines in green, in red, in magenta, in black, in pink, in purple, in blue and in dark green represent the $M_{\text{BH}} - \sigma$ relations through the quiescent galaxies in Savorgnan & Graham (2015), in McConnell & Ma (2013), in Kormendy & Ho (2013), and through the RM AGNs in Woo et al. (2015), the RM AGNs with classical bulges in Ho & Kim (2014), the RM AGNs with pseudobulges in Ho & Kim (2014) and the RM AGNs in Woo et al. (2013), and through the TDEs in Zhou et al. (2021), respectively. Solid circles in red, in blue and in cyan show the values for the 89 quiescent galaxies from Savorgnan & Graham (2015), the 29 RM AGNs from Woo et al. (2015) and the 12 TDEs from Zhou et al. (2021), respectively. Thick solid red line shows the best fitting results to all the objects, and thick dashed and dotted red lines show the corresponding 3σ and 5σ confidence bands to the best fitting results. If accepted the stellar velocity dispersion about $146 \pm 3 \text{ km/s}$ of SDSS J1241+2602 without considerations of AGN continuum emissions, solid triangle in dark green shows the virial BH mass of SDSS J1241+2602 determined by properties of the observed broad $H\alpha$ without considerations of any obscurations on central BLRs, solid and open triangles in purple show the virial BH mass of SDSS J1241+2602 determined by properties of the reddening corrected broad $H\alpha$ with $E(B - V) \sim 3.4$ (3σ confidence level for upper limit of broad $H\beta$) and $E(B - V) \sim 2.6$ (5σ confidence level for upper limit of broad $H\beta$), respectively.

are components related to shifted wing of narrow $H\alpha$, the line width ratio R_σ and the line flux ratio R_{flux} are about 27.6 and 4.8 of the shifted-wing related extended component to the core component of the narrow $H\alpha$ in SDSS J1241+2602. If simply assumed similar properties of the road components related to the shifted wings of the narrow $H\alpha$ as those discussed in blue-shifted components in [O III] lines of the 557 blue quasars in Zhang (2021a) with distributions of line width ratio R_σ and flux ratio R_{flux} of the broad component to the core component of [O III] $\lambda 5007\text{\AA}$ shown in Fig. 4, probability about $1.54 \times$

10^{-10} for $\log(R_\sigma) > \log(27.6)$ and probability about 1.21% for $\log(R_{flux}) > \log(4.8)$. Therefore, the probability is only about $1.54 \times 10^{-10} \times 1.21\% \sim 1.86 \times 10^{-12}$ for a shifted-wing related broad component in SDSS J1241+2602, leading to the similar virial BH mass. In other words, confidence level is higher than 5σ to support that the broad components in Balmer lines are not components related to shifted wings of narrow Balmer lines but really related to central BLRs in SDSS J1241+2602.

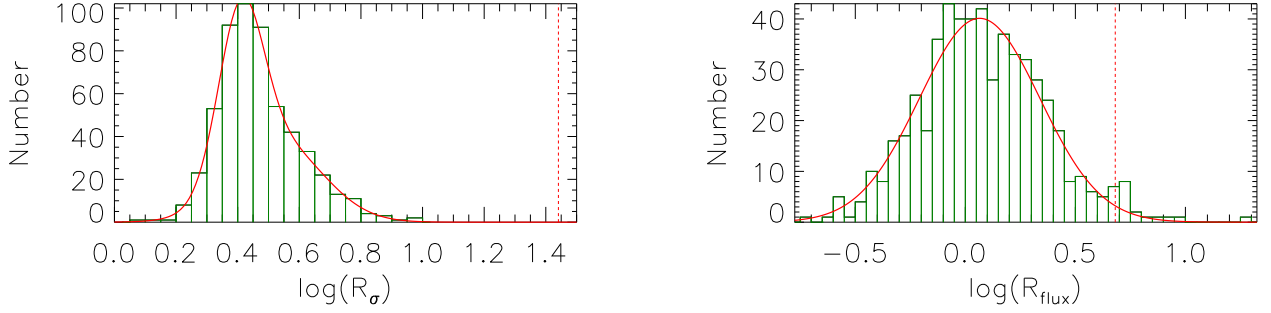


Figure 4. Distributions of $\log(R_\sigma)$ and $\log(R_{flux})$ of the shifted-wing related broad component to the core component of $[\text{O III}]\lambda 5007\text{\AA}$ of the 557 blue quasars discussed in Zhang (2021a). In each panel, solid red line shows the multiple-Gaussian-function description to the distribution, and vertical dashed red line marks position of SDSS J1241+2602.

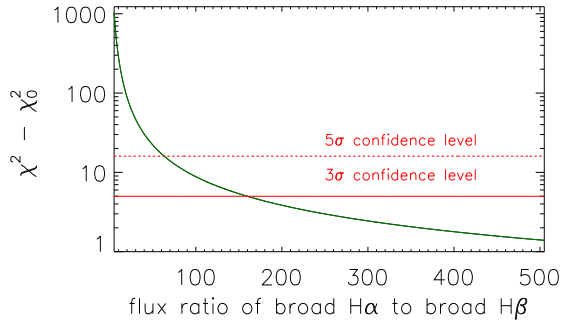


Figure 5. Dependence of $\chi^2 - \chi_0^2$ on BD_b . Horizontal solid and dotted red lines show the 3σ and 5σ confidence levels, respectively.

However, if accepted the disappearance of broad $H\beta$ was due to serious obscurations on central BLRs in SDSS J1241+2602, upper limits of line flux of the broad $H\beta$ can be simply estimated through F-test technique as follows, and then different virial BH mass can be estimated. Assumed the obscured broad $H\beta$ overwhelmed in spectral noises have the same line profile as that ($[\lambda(H\alpha_b), f_\lambda(H\alpha_b)]$) of broad $H\alpha$ described by three Gaussian functions but have total line flux determined by the line flux of broad $H\alpha$ divided by the expected broad Balmer decrement BD_b , then the intrinsic but obscured broad $H\beta$ can be described as

$$[\lambda(H\beta_b), f_\lambda(H\beta_b)] = [\lambda(H\alpha_b) \times \frac{4862.68\text{\AA}}{6564.61\text{\AA}}, \frac{f_\lambda(H\alpha_b)}{BD_b}] \quad (3)$$

For the observed line spectrum shown in top left panel of Fig. 2, contributions of obscured broad $H\beta$ can be considered, and new line spectrum can be created as

$$[\lambda(H\beta_b), f_\lambda] = [\lambda(H\beta_b), f_{\lambda, obs} + f_\lambda(H\beta_b)] \quad (4)$$

Then, for a series of 1000 new line spectrum including different contributions of obscured broad $H\beta$ with different values

of BD_b (larger than 3), χ^2 values can be calculated

$$\chi_i^2 = \sum \left(\frac{f_\lambda - Y_{fit}}{y_{err}} \right)^2 \quad (i = 1, \dots, 1000) \quad (5)$$

with Y_{fit} as the shown best fitting results in top left panel of Fig. 2 and y_{err} as uncertainties of SDSS spectrum. Then, through the F-test statistical technique applied with 1 (only one additional parameter of BD_b) and 343 ($do f_0 - 1$) as number of dofs of the F-distribution numerator and denominator, the calculated 3σ and 5σ confidence levels $CL \sim (\frac{\chi^2 - \chi_0^2}{1}) / (\frac{\chi^2}{343})$ for strong broad $H\beta$ can lead $\chi^2 - \chi_0^2$ to be 5 and 16, respectively. Here, χ_0^2 and $do f_0$ are for the best fitting results shown in top left panel of Fig. 2.

The dependence of $\chi^2 - \chi_0^2$ on BD_b is shown in Fig. 5, leading to $BD_b \sim 160$ and $BD_b \sim 64$ for the obscured broad $H\beta$ with 3σ and 5σ confidence levels, leading $E(B - V)$ to be around 3.4 and 2.6, assumed the intrinsic flux ratio 3.1 of broad $H\alpha$ to broad $H\beta$. Therefore, considering serious obscurations on central BLRs with $E(B - V) \sim 3.4$ ($E(B - V) \sim 2.6$), the reddening corrected line luminosity of the broad $H\alpha$ should be about 1605 (283) times higher than the value from the observed broad $H\alpha$, leading the reddening corrected virial BH mass to be about 58 (22) times higher than the value from properties of the observed broad $H\alpha$. The corrected virial BH masses are shown as solid/open five-point-stars in purple in Fig. 3, quite larger than the $M_{BH} - \sigma$ relation expected values.

In order to show more clear results in Fig. 3, the 89 quiescent galaxies from Savorgnan & Graham (2015) and the 29 reverberation mapped (RM) AGN from Woo et al. (2015) and the 12 tidal disruption events (TDEs) from Zhou et al. (2021) are considered to draw the linear correlation between stellar velocity dispersion and BH mass

$$\log\left(\frac{M_{BH}}{M_\odot}\right) = (-2.89 \pm 0.49) + (4.83 \pm 0.22) \times \log\left(\frac{\sigma_\star}{\text{km/s}}\right) \quad (6)$$

through the Least Trimmed Squares robust technique (Cappellari et al. 2013). And then the 3σ and 5σ confidence

bands to the linear correlation are determined and shown in Fig. 3. Therefore, the reddening corrected virial BH mass should lead the SDSS J1241+2602 as an outlier with confidence levels higher than 5σ .

Before end of the section, one point is noted. As shown in Section 3, large stellar velocity dispersion $\sim 146\text{km/s}$ can be estimated in SDSS J1241+2602, if not considering AGN continuum emissions apparently included in the SDSS spectrum. It is necessary to discuss whether the larger stellar velocity dispersions can affect our final results shown in Fig. 3. Here, we consider the question by the following two points. On the one hand, the F-test technique can be applied to confirm the confidence level higher than 5σ for the AGN continuum emissions described by the 5th-order polynomial function included in model functions to describe the SDSS spectrum of SDSS J1241+2602, based on the $\chi^2/dof = 3272.56/3382 \sim 0.96$ and the $\chi^2/dof = 3972.38/3387 \sim 1.17$ for the SSP method determined best descriptions to the SDSS spectrum with and without considerations of AGN continuum emissions. Therefore, the stellar velocity dispersion $\sim 110\text{km/s}$ is preferred in SDSS J1241+2602, considering contributions of AGN continuum emissions to the SDSS spectrum. On the other hand, even without considerations of AGN continuum emissions, properties of SDSS J1241+2602 with the larger stellar velocity dispersion about $146 \pm 3\text{km/s}$ are also shown in Fig. 3 as triangles in different colors, to re-support that the reddening corrected virial BH mass can also lead the SDSS J1241+2602 to be a unique outlier in the space of virial BH mass versus stellar velocity dispersion. Therefore, different stellar velocity dispersions with and without considerations of AGN continuum emissions have few effects on our final conclusions.

Considering the $M_{\text{BH}} - \sigma$ relation (no effects from obscurations on central BLRs) expected BH mass, the heavily obscured central BLRs should be disfavoured in SDSS J1241+2602, indicating unobscured BLRs in the Type-1.9 AGN SDSS J1241+2602 with apparent broad $\text{H}\alpha$ but no broad $\text{H}\beta$. Besides the SDSS J1241+2602 discussed in the manuscript, H1320+551 is the other individual Type-1.9 AGN reported in the literature (Barcons et al. 2003) with unobscured BLRs. Unfortunately, there is no clear information of stellar velocity dispersion in H1320+551, leading to no further discussions on BH mass properties determined through different methods as discussed in the manuscript. But in the

near future, it is interesting to check virial BH mass properties of a large sample of Type-1.9 AGN, to test whether unobscured BLRs are common in Type-1.9 AGN, and then to provide clues on evolution of different Types of AGN under the framework of the AGN unified model..

5. CONCLUSIONS

Based on the measured stellar velocity dispersion through the absorption features in the Type-1.9 AGN SDSS J1241+2602 with apparent broad $\text{H}\alpha$ but no broad $\text{H}\beta$, the $M_{\text{BH}} - \sigma$ relation expected BH mass is consistent with the virial BH mass through the observed broad $\text{H}\alpha$ without considering any obscurations on central BLRs. Meanwhile, if considering serious obscurations on central BLRs to explain the disappearance of broad $\text{H}\beta$ in the Type-1.9 AGN SDSS J1241+2602, the reddening corrected broad $\text{H}\alpha$ line luminosity should lead SDSS J1241+2602 having the re-calculated reddening corrected virial BH mass to be an outlier in the $M_{\text{BH}} - \sigma$ space with confidence level higher than 5σ . Based on the properties of virial BH mass, the unobscured central BLRs is favoured in the Type-1.9 AGN SDSS J1241+2602. The results indicate that obscured/unobscured BLRs of Type-1.9 AGN should be firstly discussed, when to test the AGN unified model by properties of Type-1.9 AGN.

ACKNOWLEDGEMENTS

Zhang gratefully acknowledge the anonymous referee for giving us constructive comments and suggestions to greatly improve our paper. Zhang gratefully acknowledges the research funding support from GuangXi University and the kind funding support from NSFC-12173020 and NSFC-12373014. This research has made use of the data from the SDSS (<https://www.sdss.org/>) funded by the Alfred P. Sloan Foundation, the Participating Institutions, the National Science Foundation and the U.S. Department of Energy Office of Science. The research has made use of the MPFIT package <https://pages.physics.wisc.edu/~craigm/idl/cmpfit.html> to solve the least-squares problem through the Levenberg-Marquardt technique, and of the LTS_LINEFIT package <https://www-astro.physics.ox.ac.uk/~cappellari/software/> to do linear fitting through Least Trimmed Squares robust technique.

REFERENCES

- Antonucci, R., 1993, ARA&A, 31, 473
- Batiste, M.; Bentz, M. C.; Raimundo, S. I.; Vestergaard, M.; Onken, C. A., 2017, ApJL, 838, 10
- Bennert, V. N.; Treu, T.; Ding, X.; et al., 2021, ApJ, 921, 36
- Balokovic, M.; Brightman, M.; Harrison, F. A.; et al., 2018, ApJ, 854, 42
- Barcons, X.; Carrera, F. J.; Ceballos, M. T., 2003, MNRAS, 339, 757
- Bentz, M. C.; Denney, K. D.; Grier, C. J, et al., 2013, ApJ, 767, 149

- Bornancini, C.; Garcia Lambas, D., 2020, MNRAS, 494, 1189
- Bruzual, G.; Charlot, S. 2003, MNRAS, 344, 1000
- Canfield, R. C.; Puetter, R. C., 1981, ApJ, 243, 390
- Cappellari, M.; Scott, N.; Alatalo, K., et al., 2013, MNRAS, 432, 1709
- Cappellari, M., 2017, MNRAS, 466, 798
- Cid Fernandes, R.; Mateus, A.; Sodre, L.; Stasinska, G.; Gomes, J. M., 2005, MNRAS, 358, 363
- Ferrarese, F.; Merritt, D., 2000, ApJL, 539, 9
- Franceschini, A.; Braito, V.; Fadda, D., 2002, MNRAS Letter, 335, 51
- Gebhardt, K.; Bender, R.; Bower, G., et al., 2000, ApJL, 539, 13
- Greene, J. E.; Ho, L. C., 2005, ApJ, 630, 122
- Goodrich, R. W., 1990, ApJ, 355, 88
- Graham, A. W.; Onken, C. A.; Athanassoula, E.; Combes, F. 2011, MNRAS, 412, 2211
- Ho, L. C.; Kim, M.-J., 2014, ApJ, 789, 17
- Hernandez-Garcia, L.; Masegosa, J.; Gonzalez-Martin, O.; Marquez, I.; Guainazzi, M.; Panessa, F., 2017, A&A, 602, 65
- Heckman, T. M.; Best, P. N., 2014, ARA&A, 52, 589
- Kauffmann, G.; Heckman, T. M.; Tremonti, C., et al. 2003, MNRAS, 346, 1055
- Kwan, J.; Krolik, J. H., 1981, ApJ, 250, 478
- Kormendy, J.; Ho, L. C., 2013, ARA&A, 51, 511
- Kuraszkiewicz, J.; Wilkes, B. J.; Atanas, A.; et al., 2021, ApJ, 913, 134
- Liu H.-Y., Liu W.-J., Dong X.-B., Zhou H., Wang T., Lu H., Yuan W., 2019, ApJS, 243, 21
- Martin-Navarro, I.; Shankar, F.; Mezcuca, M., 2022, MNRASL, 513, 10
- McConnell, N. J.; Ma, C. P., 2013, ApJ, 764, 184
- Mejia-Restrepo, J. E.; Trakhtenbrot, B.; Koss, M. J., et al., 2022, ApJS, 261, 5
- Moran, E. C.; Barth, A. J.; Kay, L. E.; Filippenko, A. V., 2020, ApJL, 540, 73
- Netzer, H., 2015, ARA&A, 53, 365
- Oh, K.; Yi, S. K.; Schawinski, K.; Koss, M.; Trakhtenbrot, B.; Soto, K., 2015, ApJS, 219, 1
- Onken, C. A.; Ferrarese, L.; Merritt, D.; Peterson, B. M.; Pogge, R. W.; Vestergaard, M.; Wandel, A., 2004, ApJ, 615, 645
- Osterbrock, D. E., 1981, ApJ, 249, 462
- Osterbrock, D. E.; Mathews, W. G., 1986, ARA&A, 24, 171
- Park, D.; Kelly, B. C.; Woo, J.-H.; Treu, T., 2012, ApJS, 203, 6
- Peterson, B. M.; Ferrarese, L.; Gilbert, K. M., et al., 2004, ApJ, 613, 682
- Savic, D.; Goosmann, R.; Popovic, L. C.; Marin, F.; Afanasiev, V. L., 2018, A&A, 614, 120
- Savorgnan, G. A. D.; Graham, A. W., 2015, MNRAS, 446, 2330
- Shen, Y.; Richards, G. T.; Strauss, M. A.; et al., 2011, ApJS, 194, 45
- Sulentic, J. W.; Marziani, P.; Dultzin-Hacyan, D., 2000, ARA&A, 38, 521
- Tran, H. D., 2003, ApJ, 583, 632
- Vanden Berk, D. E.; Richards, G. T.; Bauer, A.; et al., 2001, AJ, 122, 549
- Vestergaard, M., 2002, ApJ, 571, 733
- Villarroel, B.; Korn, A. J., 2014, Nature Physics, 10, 417
- Woo, J.-H.; Treu, T.; Barth, A. J.; et al., 2010, ApJ, 716, 269
- Woo, J.-H., Schulze, A.; Park, D.; Kang, W.; Kim, S. C.; Riechers, D. A., 2013, ApJ, 772, 49
- Woo, J.-H.; Yoon, Y.; Park, S.; Park, D.; Kim, S. C., 2015, ApJ, 801, 38
- Zhang, X. G., 2021, MNRAS, 502, 2508
- Zhang, X. G., 2021a, ApJ, 909, 16, ArXiv:2101.02465
- Zhang, X. G., 2021b, ApJ, 919, 13, ArXiv:2107.09214
- Zhang, X. G., 2022a, ApJS, 260, 31
- Zhang, X. G., 2022b, ApJS, 261, 23
- Zhang, X. G., 2022c, ApJ, 937, 105, ArXiv:2209.02164
- Zhou, Z. Q.; Liu, F. K.; Komossa, S., et al., 2021, ApJ, 907, 77
- Zou, F.; Yang, G.; Brandt, W. N.; Xue, Y., 2019, ApJ, 878, 11